Focused-ion-beam induced interfacial intermixing of magnetic bilayers for nanoscale control of magnetic properties

2014 J. Phys.: Condens. Matter 26 236002

(http://iopscience.iop.org/0953-8984/26/23/236002)

OPEN ACCESS
IOP Publishing
Made open access 12 December 2014
Journal of Physics: Condensed Matter
J. Phys.: Condens. Matter **26** (2014) 236002 (9pp)
doi:10.1088/0953-8984/26/23/236002

Focused-ion-beam induced interfacial intermixing of magnetic bilayers for nanoscale control of magnetic properties

D M Burn[1], T P A Hase[2] and D Atkinson[1]

[1] Department of Physics, University of Durham, Durham, DH1 3LE, UK
[2] Department of Physics, University of Warwick, Coventry CV4 7AL, UK

E-mail: del.atkinson@durham.ac.uk

Received 30 January 2014, revised 21 March 2014
Accepted for publication 14 April 2014
Published 16 May 2014

Abstract

Modification of the magnetic properties in a thin-film ferromagnetic/non-magnetic bilayer system by low-dose focused ion-beam (FIB) induced intermixing is demonstrated. The highly localized capability of FIB may be used to locally control magnetic behaviour at the nanoscale. The magnetic, electronic and structural properties of NiFe/Au bilayers were investigated as a function of the interfacial structure that was actively modified using focused Ga^+ ion irradiation. Experimental work used MOKE, SQUID, XMCD as well as magnetoresistance measurements to determine the magnetic behavior and grazing incidence x-ray reflectivity to elucidate the interfacial structure. Interfacial intermixing, induced by low-dose irradiation, is shown to lead to complex changes in the magnetic behavior that are associated with monotonic structural evolution of the interface. This behavior may be explained by changes in the local atomic environment within the interface region resulting in a combination of processes including the loss of moment on Ni and Fe, an induced moment on Au and modifications to the spin-orbit coupling between Au and NiFe.

Keywords: magnetic thin-film, bilayer, interfacial intermixing, interface, focused ion beam

(Some figures may appear in colour only in the online journal)

1. Introduction

Nanoscale control of the properties of functional materials is required in many applications. For magnetic materials, lithographic patterning of the two dimensional shape of magnetic structures has been widely used to modify and control the magnetization behavior. For example patterning has been used to create shape-induced anisotropies for memory and sensor applications and by controlling the localized nanoscale features, the pinning and propagation behavior of magnetic domain walls in nanowire-based data storage concepts has been demonstrated. However, such lithographic processes present issues of scalability when moving to ever smaller structures and the resulting magnetic behavior can be very sensitive to small-scale defects or local variations in structure which resulting from the lithography process. Therefore, new and alternative routes to nanoscale control of magnetic properties are needed with an enhanced understanding of the processes involved.

Magnetic moments originate from the electronic structure of the atom due to the subtle interplay between the orbital and spin contributions of its electrons. As such, they offer a direct route to probe the underlying electronic structure of a material as any modifications of the magnetic moment reflects an underlying change in the electronic structure. A detailed understanding of how the spin and orbital contributions can be effected in a material are of fundamental and technological interest as they underpin much of modern technology. Controllable changes in the magnetic properties of a material allow the development of the next generation of magnetic and spintronic devices to be realized. By careful tailoring of the material properties (i.e. the electronic structure) devices can be conceived in which information can be stored in magnetic materials leading to applications such as magnetic memory

[1, 2] and or logic [3]. Advances in patterning techniques with the concomitant ability to perform material modification on the nanoscale has opened up new technological opportunities in magnetic materials, but the affect of the patterning processes on the electronic structure of the patterned material remains only partially understood.

Focused-ion-beam irradiation is a highly advantageous and versatile tool for nanoscale device fabrication and relies on impinging ions to modify the surface either through the direct removal of material, ion-implanation or modification of the electronic structure. The interaction of the ions with a material is strongly dependent on the ion species, its energy and overall dose. In certain thin multilayered magnetic systems such as Co/Pt multilayers a strong perpendicular magnetic anisotropy (PMA) results from magnetoelastic effects due to symmetry breaking at the sharp interfaces [4]. Chappert [5] showed how interfacial intermixing from broad-beam He^+ ion irradiation can remove this interfacial anisotropy and modify the dominant anisotropy of these films, driving the magnetisation into the plane. In other material systems, such as permalloy (nominal composition $Ni_{81}Fe_{19}$), there are no strong interfacial anisotropy contributions so the anisotropy is governed simply by the geometry of the film and is typically in-plane. However, upon direct ion irradiation a decrease in the saturation magnetization of the near-surface region has been observed [6] which eventually renders the surface nonmagnetic [7–10]. This effect is coupled with an increasing coercivity with dose that is attributed to several phenomena including ion-induced damage of the crystal structure, the introduction of scattering defects within the thin-film and the emergence of lattice stress from the inclusion of the large impurity ions [11, 12]. These previous works have tended to focus on the high dose regime where damaging effects of the ion irradiation can be observed clearly. However, more subtle changes in material properties that occur in the low dose regime where intermixing effects dominate have so far been overlooked.

Here we show how Ga^+ ion irradiation of NiFe/Au bilayers with in-plane magnetization is modified by low dose focused-ion-beam irradiation. The aim being to gain insight into the interesting behavior in a model Magnetic/Non-Magnetic bilayer driven by interfacial intermixing. The material system was chosen because permalloy is the archetypal magnetic material that has been used in many previous in-plane studies of thin-films and nanostructures. A second consideration is that Au is often used as protective capping layer to limit oxidation, and being chemically unreactive, the physical effects of ion-irradiation are unlikely to be complicated by the formation of additional chemical phases when intermixed with the adjacent layer. The electron density contrast between Au and both Ni and Fe is also advantageous for the x-ray methods used for the structural analysis described herein.

The modification of magnetic moments due to the local environment of an introduced atomic species has previously been observed for pure Ni and pure Fe when alloyed, or interfaced to a non-magnetic atomic species [13]. Indeed, induced magnetic moments on Au can arise from proximity with other 3*d* ferromagnets [14–16] and spontaneous moments have even been identified from purely geometrical effects in ultrasmall pure Au nanoparticles [17–20]. We will show here that in our NiFe/Au bilayer system irradiation gives rise to dramatic changes in the magnetic properties as a function of irradiation dose at much lower doses than those needed to modify the magnetic properties in pure NiFe. Analysis of the magnetic properties through x-ray magnetic circular dichroism (XMCD) and anisotropic magnetoresistance (AMR) measurements give insight into the changes in magnetic moment as the interfacial intermixed region develops. A variety of potential physical mechanisms that may explain the observed effects are discussed in terms of subtle modifications to the interface between NiFe and Au, where the low dose ion irradiation introduces local intermixing that gives rise to a compositionally graded alloy layer centred at the interface [21, 22].

2. Experimental details

Permalloy thin films (nominally $Ni_{81}Fe_{19}$), capped with Au, were prepared by thermal evaporation onto either Si substrates with a 500 nm hydrothermally oxidised SiO_2 layer or 200 nm thick SiN windows in a single growth cycle without breaking vacuum. The base pressure was of the order 5×10^{-7} Torr rising to $1 - 4 \times 10^{-6}$ Torr during deposition. The layer thicknesses and rate of deposition were monitored with an in-situ quartz rate monitor that was previously calibrated using x-ray reflectivity.

To ensure any observed variations between samples were attributable to changes in the ion dose, a series of e-beam lithographically patterned elements were created on a single substrate. For magneto-optical Kerr effect (MOKE) magnetometry studies, well separated arrays of elliptical structures ($50 \times 10\ \mu$m) were created by lift-off allowing a wide range of Ga^+ irradiation doses to be systematically explored. For characterization techniques which required larger surface areas the layers were deposited through a set of shadow masks to create several patterned regions of 1×1.5 mm and 1.3×5.5 mm. The structures were then irradiated at normal incidence using 30 keV Ga^+ ions focussed to an approximately 20 nm spot using a FEI Helios NanoLab 600 FIB system. The beam was rastered over a $100 \times 50\ \mu$m area which enclosed the elliptical structures of the MOKE study. For the larger samples, the ion beam was rastered over 100 or 200 μm write fields followed by a movement of the stage and subsequent exposures thereby covering the entire strip. The stitching error associated with the stage movements was negligible in comparison to the footprint of the experimental probes. Irradiation doses ranging from 0.1×10^{15} Ga cm^{-2} to 13.0×10^{15} Ga cm^{-2} were controlled by the number of repeat exposures of each pixel for a set dwell time of 1 μs with a 50% pixel overlap.

A focused MOKE system was used to probe the elliptical structures to determine both the coercivity and the relative Kerr signal intensity for a wide range of irradiation doses. In these measurements the MOKE polling direction was aligned with the long axis of the ellipse and with a ±300 Oe sinusoidal magnetic field applied at 27 Hz. The MOKE response was averaged over many field cycles for approximately 1 min to improve the signal-to-noise ratio of the data. Further investigation of the magnetic properties were then performed on

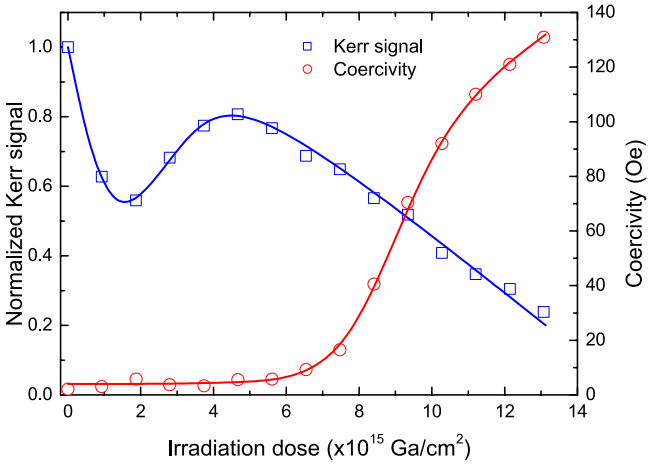

Figure 1. Coercivity and normalized Kerr signal as a function of Ga^+ irradiation dose on NiFe (10 nm)/Au (7 nm) ellipses. The Kerr signal shows a general linear decrease but has a pronounced dip followed by a recovery at low doses. At low doses the material has a small and consistent coercivity which rises at higher doses until beyond 13×10^{15} Ga cm^{-2} the MOKE loop could not be measured.

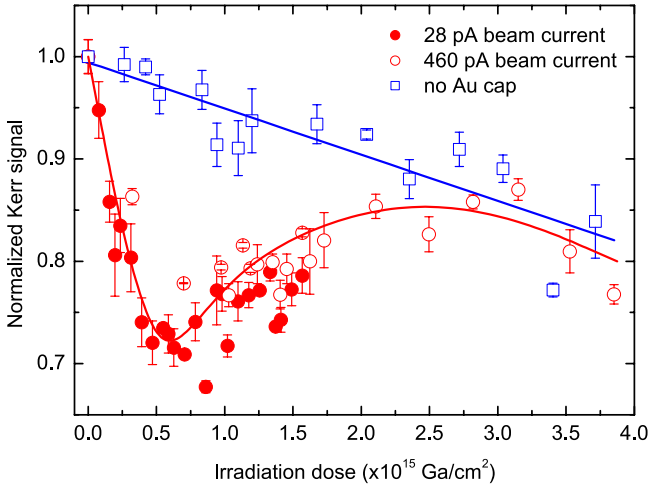

Figure 2. Normalised Kerr signal as a function of Ga^+ dose for NiFe (15 nm) ellipses, with and without a Au (2.5 nm) cap. The uncapped samples show a linear dependence with dose whilst the Au capped samples show a dip and recovery which is independent on current.

the larger (1.3 × 5.5 mm, 20 nm NiFe/2.5 nm Au) samples at selected irradiation doses using superconducting quantum interference device (SQUID) measurements to give a quantitative measure of the magnetic moment of the samples. Hysteresis loops were recorded at 290 K with magnetic field sweeping ±30 Oe along the long axes of the samples. The paramagnetic contribution from a blank substrate was measured and the response subtracted. X-ray magnetic circular dichroism (XMCD) measurements were used to probe the element specific magnetic moment contributions from Ni and Fe as a function of irradiation dose. These measurements were performed in transmission mode using the 1 × 1.5 mm, 20 nm NiFe/2.5 nm Au structures on SiN windows. Differences in the dichoric x-ray absorption were measured at the Fe and Ni $L_{3,2}$ edges using circularly polarized x-rays generated from an elliptically polarizing undulator at the ID1011 beamline at MAX-lab [23]. The spectra were analyzed using the sum rules [24] giving the ratio of the orbital to spin moments for both Fe and Ni as a function of irradiation dose. Magnetoresistance measurements were performed in a four point geometry at room temperature with a 1 mA direct current applied along the long axis of the 1.3 × 5.5 mm samples. An applied magnetic field was swept ±500 Oe both parallel and perpendicular to the current direction. The resistance data were corrected to remove any thermal drift from Ohmic heating in the samples. The structure of the interface was also investigated through grazing incidence x-ray reflectivity (GIXR) measurements at the XMaS beamline at the ESRF, Grenoble, France. Full details of the experimental procedure and analysis of the interface width as a function of irradiation dose can be found in our previous work [25]. In this paper, we extend the structural analysis to elucidate the nature of the interfaces in terms of the contributions from chemical intermixing and topological roughness. This was determined from measurements of the diffuse scatter which was recorded by rocking the sample at a fixed scattering angle, 2θ. The structural results are further supported with TRIDYN simulations of ion-target interactions [26]. These simulations estimate the change in the atomic profiles through the film as a function of the incident ion beam energy by considering the interaction of the ion energy on the local bonding within the sample [27, 28].

3. Results

3.1. MOKE

For all the magnetic structures discussed here the MOKE hysteresis loops showed magnetic saturation well below the 300 Oe maximum field used in the measurements. The variation in Kerr signal and coercivity as a function of Ga^+ irradiation dose for 10 nm NiFe/7 nm Au bilayer elliptical structures prepared on a single substrate are shown in figure 1. The coercivity is low for the unirradiated sample, which is typical for thin-film permalloy and remains constant for irradiation doses below 7×10^{15} Ga cm^{-2}. At this point the coercivity begins to rise which may be attributed to an increasing defect density within the film leading to enhanced domain wall pinning [11]. In this high-dose region the decrease in Kerr signal indicates a degradation in the magnetic properties and the eventual formation of a ferromagnetic dead layer beyond a dose of 13×10^{15} Ga cm^{-2}. This is consistent with previous work on similar materials [7]. More interesting is the rapid fall, followed by a recovery in the Kerr signal intensity in the low-dose regime shown in figure 1 without any obvious changes in the coercivity. This anomalous behavior is the focus of this work.

Further MOKE measurements concentrating on this low dose regime are shown in figure 2 for a bilayer with a thicker ferromagnetic layer (15 nm NiFe) and a thinner (2.5 nm Au) capping layer. The same trend seen in figure 1 is also observed in these samples. Figure 2 also compares irradiated structures with and without the Au cap. This comparison highlights the fact that the complex low dose magnetisation behavior occurs only in the presence of the capping layer. Furthermore, replacing the Au with a Cu capping layer also shows similar behaviour (data not shown). The changes in the magnetization in the

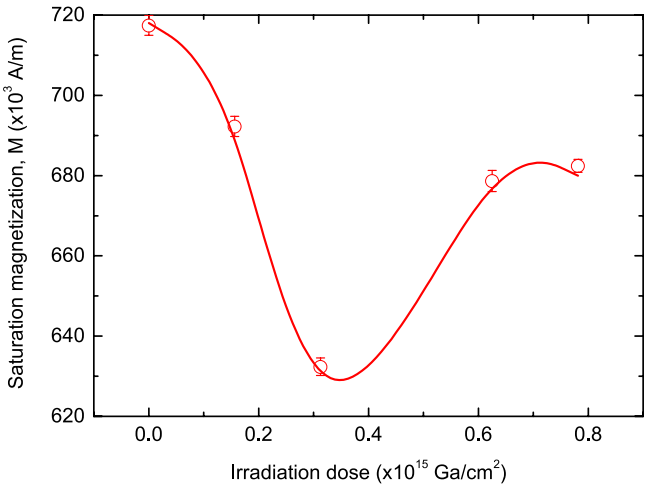

Figure 3. Variation of M_S with dose for 1.3 × 5.5 mm 20 nm NiFe/2.5 nm Au samples measured using SQUID magnetometry which show a drop followed by a recovery in the magnetic moment. The line is a guide to the eye.

low-dose regime for the capped samples cannot be explained by considering the effect of direct Ga^+ implantation or irradiation induced damage described in early high-dose work [6–11] as this would also result in changes in the uncapped samples. It is also worth noting that using either a 28 pA or 460 pA beam current for the irradiation makes no significant difference to the observed behaviour (figure 2) suggesting that the rate of irradiation which could lead to differences based on sample heating [29, 30] is also not an important parameter. Therefore the magnetization behavior observed in figure 2 must arise from a different physical process with the energy or momentum supplied by the irradiation a key parameter.

Figure 2 shows that for the thinner 2.5 nm Au cap there is a shift in the complex magnetization behavior towards lower doses in comparison with the thicker 7 nm thick Au cap data shown in figure 1. The thinner capping layer provides less attenuation of the Ga^+ beam allowing the same effect at the interface to be achieved with a lower irradiation dose. A sample thickness argument can also explain the relative size of the initial drop in the Kerr signal between these samples; the thinner 10 nm NiFe layer in figure 1 shows a 45% decrease in the Kerr signal compared to only a 30% decrease for the 15 nm NiFe layer in figure 2.

3.2. SQUID

SQUID measurements were undertaken on larger area bilayer samples of 20 nm NiFe/2.5 nm Au with selected doses to obtain a quantitative measure of the irradiation induced changes in magnetic moment and are shown in figure 3. The drop and recovery observed in the saturation magnetization as a function of dose confirms the magnetic origin of the complex behavior rather than any unrelated magneto-optical effect, change in surface reflectivity or sample alignment issues that could occur as artifacts in the MOKE measurements. The magnetic moment minimum occurs at a similar dose to that observed from the MOKE measurements in figure 2 with the same capping thickness. The relative decrease in moment obtained from SQUID measurements for the 20 nm thick NiFe layer is smaller than that obtained from the 10 nm and 15 nm data films using MOKE. As discussed later, this can be attributed to a combination of the film thickness and also to the influence of the skin-depth in the MOKE measurements. Although the entire magnetic thickness lies within the MOKE skin depth of between ∼10 − 20 nm [31], the MOKE intensity from the surface region is enhanced relative to the deeper part of the film and hence the MOKE intensity variation is weighted towards the interfacial region compared to SQUID data which averages the entire sample volume.

3.3. X-ray magnetic circular dichroism

The orbital and spin contributions to the magnetic moment were investigated through element specific x-ray magnetic circular dichroism (XMCD) measurements. The upper panel of figure 4 shows the x-ray absorption spectra (XAS) across the Fe $L_{3,2}$ edges for an unirradiated 20 nm NiFe/2.5 nm Au sample measured in a saturating magnetic field for opposite helicities of circularly polarized x-rays. The absorption peaks at the L edges shows a dichoric effect with photon helicity which was used to determine the XMCD. Applying the sum rules to the cumulative integral of the XMCD signal allows the ratio of orbital to spin magnetic moments to be determined. This ratio is shown in the lower panel of figure 4 as a function of ion dose and is around 0.2 for both the Ni and Fe with some variation in the low dose irradiation regime. Whilst noisy in the Ni data, the Fe clearly shows a feature similar to that observed in the MOKE and SQUID data. For both Ni and Fe the lowest value for the spin to orbit ratio occurs at a dose of 0.5 × 10^{15} Ga^+ cm^{-2}, the same value observed using the other techniques. Assuming a constant spin contribution this suggests an enhancement in orbital quenching in the low-dose regime due to a modification to the spin-orbit coupling.

3.4. Magnetoresistance

An alternative probe of the spin–orbit interaction is through the anisotropic magnetoresistance (AMR) effect. The AMR ratio is defined: $AMR = \frac{\Delta R}{R_{av}}$, where $\Delta R = R_{\parallel} - R_{\perp}$ is the difference in resistance between the parallel ($R_{\parallel}$) and perpendicular ($R_{\perp}$) magnetic geometries and $R_{av} = \frac{1}{3}R_{\parallel} + \frac{2}{3}R_{\perp}$ is the baseline resistance of the sample. Figure 5 shows the variation in both the baseline resistance and AMR as a function of irradiation dose. The peak in the AMR ratio coincides with the minimum in the magnetic moment (figure 3) and contrasts with the steady increase in baseline resistance over this dose range. The increase in baseline resistance may arise from a slight reduction in Au thickness through sputtering of the Au layer by the Ga^+ or it may be due to an increase in spin-independent scattering from defects introduced into the film by the irradiation. More importantly, the baseline resistance does not show any significant changes with dose in contrast to the peak in the magnetoresistance ratio, which suggests that the origin of the AMR peak is solely a magnetoresistive phenomenon and

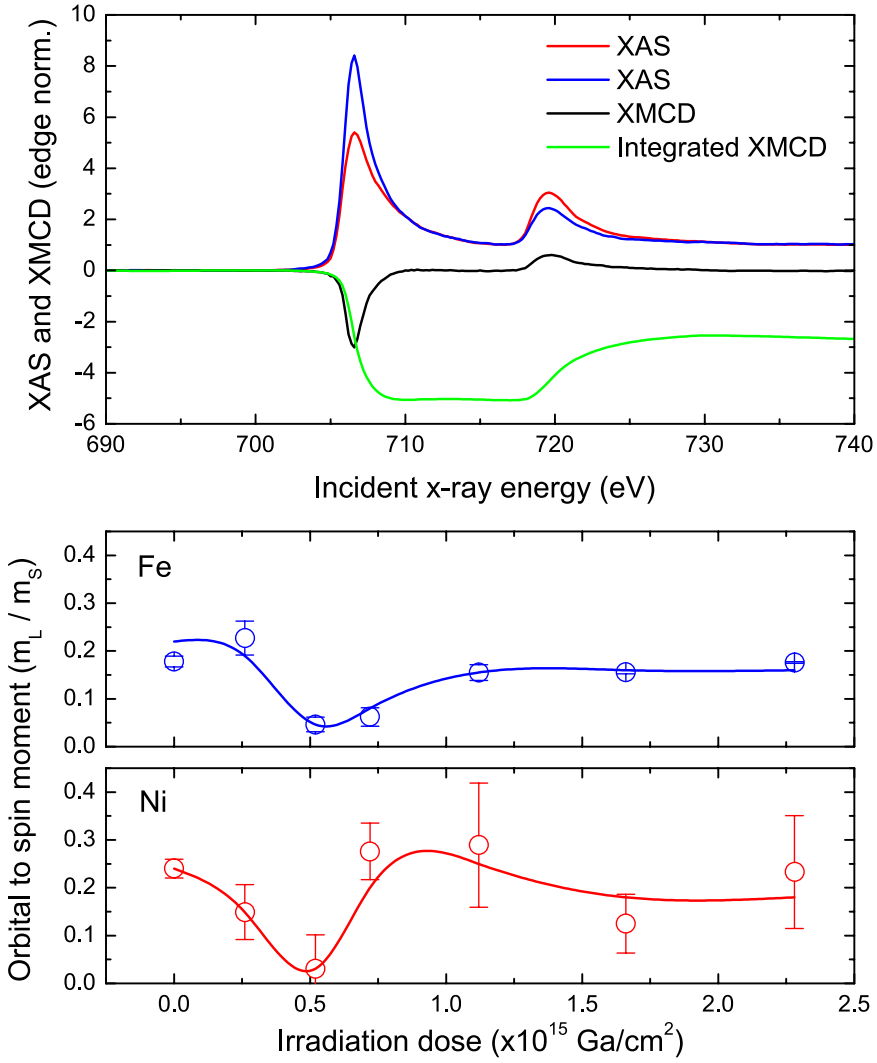

Figure 4. Top: x-ray absorption for both helicities of circularly polarized x-rays and their difference over the $L_{3/2}$ for Fe. The cumulative integral of the XMCD was used to find the ratio of the orbital to spin contributions to the magnetic moment. Bottom: orbital to spin ratio of the contribution of the magnetic moment for Ni and Fe atoms as a function of Ga^+ dose. The solid lines are a guide to the eye and highlight the dip also observed in the magnetization in the low dose regime.

hence is indicative of a change in the spin–orbit interaction in agreement with the XMCD data.

3.5. Interface structure

Alongside the magnetic analysis of these samples, TRIDYN simulations on a NiFe/Au bilayer were performed with a model comprising a 3 nm Au cap on top of a thick NiFe layer to investigate the structural changes as a function of Ga^+ dose. Figure 6 shows simulated depth profiles of the relative atomic composition from the surface of the sample after various doses of irradiation. An initially sharp simulated interface at the 3 nm position becomes broadened by intermixing resulting from the low-dose irradiation. Estimates of the interface width were obtained from the width over which the composition varied from 5% to 95% and the square of this interface width was found to vary linearly with Ga^+ dose (not shown). The TRIDYN results are in excellent agreement with experimental

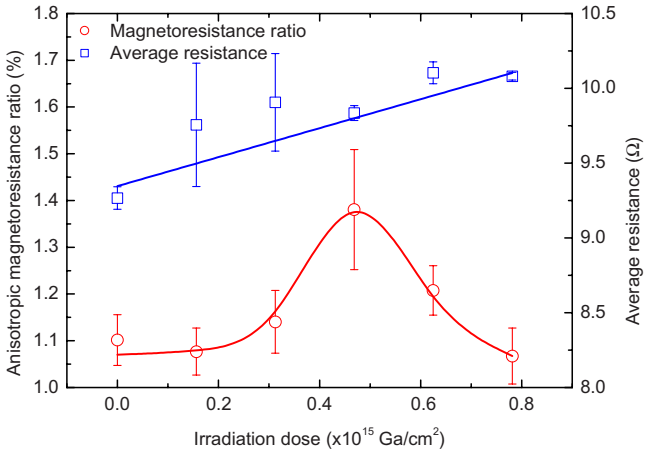

Figure 5. Anisotropic magnetoresistance ratio and baseline resistance of 20 nm NiFe/2.5 nm Au bilayers as a function of Ga^+ irradiation dose. The solid lines represent a linear fit to the average resistance data and a guide to the eye for the AMR data.

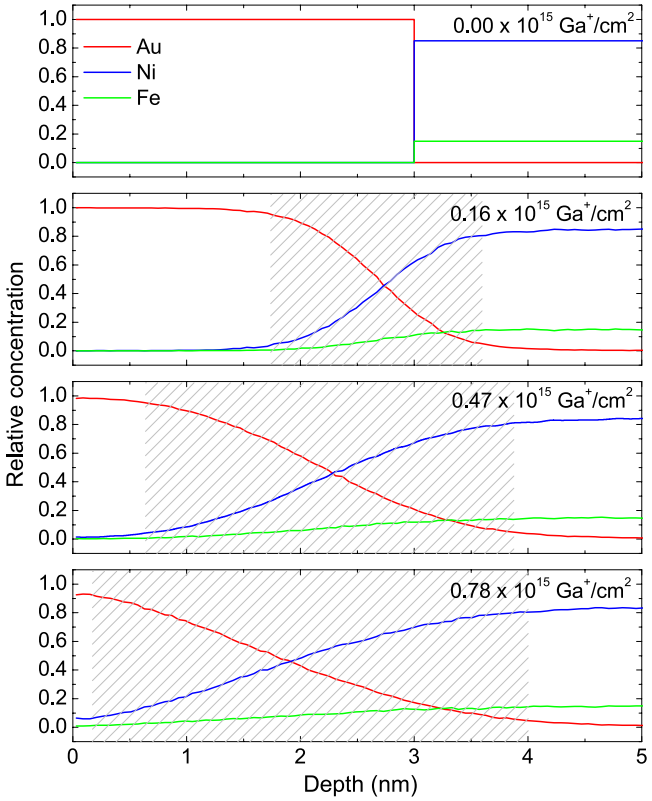

Figure 6. TRIDYN simulations of the depth dependent composition through the interfaces of a 3 nm Au cap on a NiFe slab. The gray shaded region represents the increasing interface width with dose.

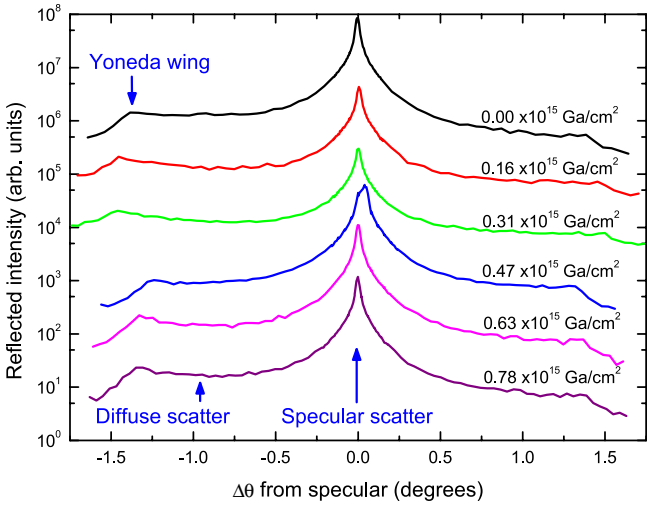

Figure 7. Rocking curves ($\Delta\theta$) recorded at a Keissig maximum as a function of Ga^+ dose. The specular scatter is located at $\theta = 0$ with the critical angles marked by the Yoneda wings which are symmetrically positioned either side of the specular ridge. Curves are offset for clarity.

measurements of the interface width deduced from fitting the specular x-ray reflectivity [25]. The structure of the interface can be deconvolved into two components. One describes the topological roughness, or morphology of the interface, and the second represents the interfacial intermixing of the two layers. The relative contribution of these two components can be quantified through analysis of the diffuse scatter (figure 7). The rocking curves show

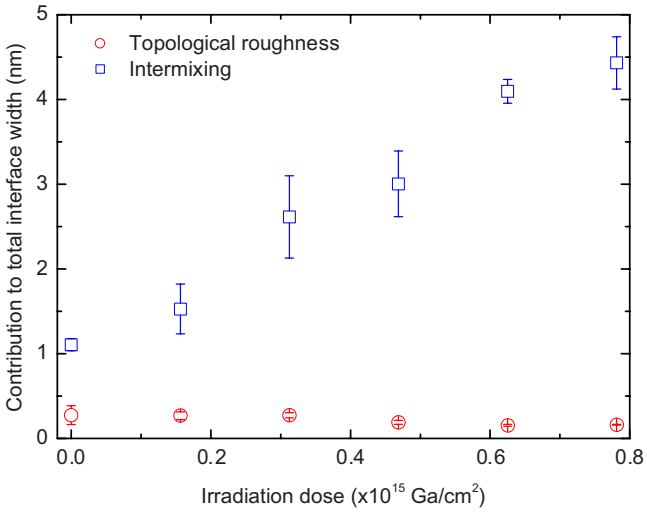

Figure 8. Differentiation between roughness and intermixing contributions to the interface width shows a constant roughness contribution and an increasing interface width that is accounted for by an increase in the chemical intermixing.

a specular peak on top of a broad diffuse background. It is only the topological roughness that contributes to this scatter. The intermixing contribution to the interface width σ_i, is then obtained from the total interface width, σ determined from the fit to the specular reflectivity using the relation: $\sigma = \sqrt{(\sigma_i^2 + \sigma_r^2)}$ where σ_r is the roughness contribution found from the ratio of the areas under the specular and diffuse regions of the curve [32]. The two contributions to the interfacial width obtained from this analysis are shown in figure 8 as a function of irradiation dose. The Ga^+ dose does not affect the topological roughness, instead the increasing width observed as a function of dose in the specular reflectivity data and the TRIDYN simulations is associated with an increase of interfacial alloying which is seen to vary linearly.

4. Discussion

MOKE and SQUID results both show a complex change in the magnetic properties of NiFe/Au bilayer structures as a function of low dose Ga^+ irradiation. The reduction in magnetization depends upon the thickness of the magnetic film, with thinner magnetic layers showing a proportionately larger change. This trend is clear from the MOKE and SQUID data, although the MOKE data is also affected by the skin-depth effect that gives a stronger response from nearer the surface than deeper into the film. This change is superimposed upon a gradual decrease in the total magnetization as a function dose, which at larger dose ranges is attributed to damage to the crystalline structure of the film [7–10]. A possible explanation of the changes in the moment under the low doses is due to sputtering of the magnetic material. However, this can be disregarded for several reasons. First the sputtering rate is very small for such low dose irradiation and results from fitting the specular reflectivity showed that the magnetic material remains enclosed within a consistent Au cap [25]. Additionally, a change in moment via sputtering would account only for a loss of material and would not explain

the subsequent recovery in moment with increasing dose. Dose dependent differential sputter rates for Ni and Fe have previously been suggested to explain changes in uncapped NiFe stoichiometry but these are with significantly higher doses [11]. Any sputtering effects are, therefore, expected to be more significant for an uncapped sample which shows only a slowly changing linear dependence and not the complex low dose behavior observed in the bilayer samples.

The addition of Ga has also been considered. First, the direct implantation of Ga ions into the magnetic material leads to the introduction of point defects, with eventual alloying at higher doses. Secondly, in Fe-Ga alloys, a decrease in moment of 0.014 μ_B/at. per % Ga has been found from the initial 2.218 μ_B per atom in Fe [33]. Similar behavior was also found for Ni-Ga alloys with a change of 0.03 μ_B/at. per % Ga [34]. Therefore, the change in moment due to the ~0.7% Ga^+ fraction predicted from TRIDYN simulations for these low doses is very small and unlikely to be significant for the magnetization changes observed here.

In contrast to the complex magnetic behavior resulting from ion beam irradiation, the structural study shows a monotonic increase in the interface width, resulting from interfacial intermixing, with no complex structural changes in the low dose regime. The complex magnetic behavior must therefore be explained as the result of a combination of physical processes occurring at the interface.

Local modifications to the electronic structure in Au and NiFe when in close proximity can lead to polarization effects, affecting the magnetic moment of both Ni and Fe and inducing a magnetic moment on the Au atoms. The moment on Ni has been seen to decrease with concentration when it forms alloys or multilayers. Examples include Ni/Pt [35, 36] Ni-mettaloid [37], NiFe/Pt [13] or NiFeTa [38] where there is an increase in the number of nonmagnetic nearest neighbors around the Ni. A decrease in moment is likely to occur when non-polarizable *p-d* hybrid bonds are formed instead of the polarizable 3*d* transition metal states [37]. The situation on the Fe sites is more complex showing an increase in fcc FeAu [14], bcc Fe(Sn, Sb, Ga, As, Ge) [37] and NiFe/Pt [13] that is attributed to volume expansion of the unit cell associated with the addition of the larger atoms [37, 39]. This interpretation also applies to the lattice contractions found with the addition of smaller adatoms such as in bcc FeB [40] and Fe(V/Cr) [41, 42] that leads to a decrease in the Fe moment. Theoretical predictions show that these volume effects lead to narrowing of the Fe 3*d* band in FeAu and an associated increase in the Fe exchange responsible for the changes in magnetic moment [43].

Atomic Au has completely filled 5*d* states, however, hybridization in its metallic form leads to a few 5*d* holes. When in proximity with 3*d* ferromagnets, exchange spin polarization can give rise to an induced magnetic moment on Au [15, 44, 45]. Such polarization is also found in other 4*d*; Ag [46], and 5*d*; W [47, 48], Ir [48] and Pt [13, 36, 49] atomic layers. The size of the induced moment in a bcc AuFe alloy increases with the number of Fe nearest neighbors, becoming a maximum when Au impurity atoms are totally surrounded by Fe atoms [14]. This induced effect diminishes with separation [15, 47]. To look for an induced moment on the Au in these bilayers we performed x-ray resonant magnetic scattering analysis at the XMaS beamline at the ESRF. The reflectivity of the bilayer in a magnetic field was investigated with circularly polarized x-rays tuned to the Au L_3 edge. This indicated a very weak magnetic dichroic signal, suggesting the presence of a small Au moment at the interfacial region.

A transfer of moment to the Au and associated hybridization of the bonds must lead to a modification of the spin–orbit ratio of the polarizing species. Further evidence for such a change in the spin-orbit interaction is obtained from the XMCD measurements at the Ni and Fe $L_{2,3}$ edges as well as via the proxy of anisotropic magnetoresistance measurements. It is suggested that the stronger spin–orbit coupling of the Au may be transferred to the magnetic atoms in a similar way to that demonstrated theoretically which would show a diminishing effect with increasing separation from the interface in layered systems [50]. Strong spin–orbit coupling was found on Au in an AuFe alloy and large exchange splitting of Fe arises from hybridization of the Au*d*–Fe*d* electronic states at an interface [45]. Experimental work has also shown the *d*-charge on Au increases with lattice expansion [51] and demonstrated an increase in magnetoresistance from the interface effects which can be explained by the stronger spin–orbit coupling of Au atoms, leading to enhanced spin-dependent scattering of the conduction electrons in NiFe [52]. Theoretical work has also demonstrated enhanced spin–orbit coupling on Fe atoms in proximity with non-ferromagnetic 5*d* atoms such as Pt [50] where the effect decreases with increasing distance from the interface in a multilayered sample [49, 50].

A combination of hybridization and moment transfer coupled with volume expansion and local Au concentration suggests an explanation for the complex behavior observed in the NiFe/Au films that is intimately linked to the development of an interfacial alloy region which forms as a function of Ga^+ dose. Consider first the induced moment on Au: During the initial stages of irradiation the NiFe layer has a low concentration of Au atoms, with each surrounded by a large number of ferromagnetic nearest neighbors. This increases the moment induced on the Au atoms and reduces the moment on Ni and perhaps Fe [14]. With further intermixing, the Au density increases and more Au atoms become polarized with a concomitant reduction in the net moment due to the local hybridization on the Ni and Fe sites. Thus, with increasing Ga^+ dose the total moment will fall. However, with further increases in Ga^+ dose the proportion of Au in the intermixed layer increases, reducing the number of ferromagnetic neighbors. This acts to re-balance the moments, reducing the induced Au moment per atom whilst simultaneously restoring the moment on the Ni and Fe and resulting in an increase in the net moment. It is thus the Au concentration in the intermixed alloy interface layer that is key in defining the resultant magnetization through its hybridization with the Ni and Fe, providing a possible explanation for the observed behavior with Ga^+ dose. A similar situation has been observed previously in NiFe/Pt multilayers where competing contributions to the magnetic moment at interfaces give rise to complex overall behavior [13]. The complex magnetization behavior with Ga^+ dose may be further complicated by the fact that the

incorporation of Au leads to an expansion of the NiFe(Au) unit cell within the intermixed layer, the effect of which is to enhance both the Fe and induced Au moments [13, 14, 37, 39, 51]. At higher doses the crystal structure is perturbed too much and the induced moment reduces and the system recovers its net moment.

Thus, the complex magnetic behavior observed in this non-magnetic/ferromagnetic bilayer system results from interfacial mixing induced by low-dose focused ion beam irradiation which results in the formation of an intermixed compositionally-graded AuNiFe alloy. Within this layer electronic hybridization and volume expansion leads to the modification of the moments of the Ni and Fe and the development of a small moment on the Au. The induced intermixing and concomitant hybridization processes evolve with the changes in the local atomic environment with increasing dose. The net result is a complex dependence on the intermixing that leads to an initial reduction followed by a recovery of the total moment as the interface alloy region expands with increasing irradiation dose. The magnetic measurements can, therefore, be understood as reflecting the combined response of a compositionally-graded interfacial AuNiFe alloy layer and any remaining NiFe layer. For a thicker NiFe layer the net change in moment of the whole sample is smaller as the interfacial layer represents a smaller volume fraction of the total. For a very thin ferromagnetic layer a larger effect would be expected.

5. Conclusions

In summary, the magnetic, electronic and structural properties of NiFe/Au bilayers have been investigated as a function of Ga^+ irradiation dose. With high dose irradiation a degradation of the magnetic properties is attributed to damage to the crystal structure of the sample. At low doses complex magnetization behavior shows a decrease followed by a recovery in the magnetic moment that is associated with interfacial intermixing between the NiFe and the Au layers. This mixing modifies the local environment of the atoms which reduces the moment on Ni and Fe due to polarization effects, increases the moment on Fe due to volume effects and leads to an induced moment on Au. There is also a modification to the spin–orbit coupling due to the interaction between the Au and NiFe atoms. Competing mechanisms have been identified, linking the change in moment with changes in the local environment. The combination of competing contributions to the magnetic properties provides an explanation for the overall complex magnetic behavior with low dose irradiation. The drop in magnetic moment is associated with an enhancement of the anisotropic magnetoresistance (AMR). The AMR peak is correlated with a reduction of the orbital moments on the Ni and Fe, indicating a linkage between the spin–orbit coupling and the spin and orbital magnetic moments.

The local control over ion beam irradiation from focused ion beam systems makes this a potentially useful technique for tuning the magnetic behavior of magnetic thin-films with low-doses, where damage to the sample surface is negligible. This method is well suited to multilayered layers and the localized modification of magnetic properties may lead to nanoscale control of the magnetic properties of materials for applications in spintronic structures, such as nanowires for memory, logic and sensing applications.

Acknowledgments

We thank L Bouchenoire (XMaS beamline, ESRF), Gunnar Öhrwall (MAX-Lab) and Matts Björck (Uppsala University) for their considerable help in facilitating the x-ray experiments. We also acknowledge the help and support of J A King, R M Rowan-Robinson, A Baker and D S Eastwood during the x-ray experiments. We are grateful to E Arac for useful discussions and thank the UK EPSRC for providing financial support. XMaS is an EPSRC funded mid-range facility managed by the Universities of Liverpool and Warwick.

References

[1] Parkin S S P, Hayashi M and Thomas L 2008 Magnetic domain-wall racetrack memory *Science* **320** 190–194
[2] Lavrijsen R, Lee J-H, Fernandez-Pacheco A, Petit D C M C, Mansell R and Cowburn R P 2013 Magnetic ratchet for three-dimensional spintronic memory and logic *Nature* **493** 647–650
[3] Allwood D A, Xiong G, Faulkner C C, Atkinson D, Petit D and Cowburn R P 2005 Magnetic domain-wall logic *Science* **309** 1688–1692
[4] Devolder T 2000 Light ion irradiation of Co/Pt systems: structural origin of the decrease in magnetic anisotropy *Phys. Rev.* B **62** 5794–5802
[5] Chappert C *et al* 1998 Planar patterned magnetic media obtained by ion irradiation *Science* **280** 1919–1922
[6] Park C-M and Bain J A 2002 Focused-ion-beam induced grain growth in magnetic materials for recording heads *J. Appl. Phys.* **91** 6830–6832
[7] Faulkner C C, Atkinson D, Allwood D A and Cowburn R P 2007 Rapid tuning of $Ni_{81}Fe_{19}$/Au bilayer magnetic properties by focused ion beam intermixing *J. Magn. Magn. Mater.* **319** 9–12
[8] Park C-M and Bain J A 2002 Local degradation of magnetic properties in magnetic thin films irradiated by Ga^+ focused-ion-beams *IEEE Trans. Magn.* **38** 2237–2239
[9] Fassbender J and McCord J 2006 Control of saturation magnetization, anisotropy, and damping due to Ni implantation in thin $Ni_{81}Fe_{19}$ layers *Appl. Phys. Lett.* **88** 252501
[10] Kaminsky W M, Jones G A C, Patel N K, Booij W E, Blamire M G, Gardiner S M, Xu Y B and Bland J A C 2001 Patterning ferromagnetism in Ni_{80} Fe_{20} films via Ga^+ ion irradiation *Appl. Phys. Lett.* **78** 1589–1591
[11] Ozkaya D, Langford R M, Chan W L and Petford-Long A K 2002 Effect of Ga implantation on the magnetic properties of permalloy thin films *J. Appl. Phys.* **91** 9937–9942
[12] Bagayoko D and Callaway J 1983 Lattice-parameter dependence of ferromagnetism in bcc and fcc iron *Phys. Rev.* B **28** 5419–5422
[13] Liu Y F, Cai J W and Sun L 2010 Large enhancement of anisotropic magnetoresistance and thermal stability in Ta/NiFe/Ta trilayers with interfacial Pt addition *Appl. Phys. Lett.* **96** 092509
[14] Wilhelm F, Poulopoulos P, Kapaklis V, Kappler J-P, Jaouen N, Rogalev A, Yaresko A N and Politis C 2008 Au and Fe

magnetic moments in disordered Au-Fe alloys *Phys. Rev.* B **77** 224414
[15] Wilhelm F, Angelakeris M, Jaouen N, Poulopoulos P, Papaioannou E T, Mueller C, Fumagalli P, Rogalev A and Flevaris N K 2004 Magnetic moment of Au at Au/Co interfaces: a direct experimental determination *Phys. Rev.* B **69** 220404
[16] Banerjee S, Raja S O, Sardar M, Gayathri N, Ghosh B and Dasgupta A 2011 Iron oxide nanoparticles coated with gold: enhanced magnetic moment due to interfacial effects *J. Appl. Phys.* **109** 123902
[17] Li C-Y, Wu C-M, Karna S K, Wang C-W, Hsu D, Wang C-J and Li W-H 2011 Intrinsic magnetic moments of gold nanoparticles *Phys. Rev.* B **83** 174446
[18] Hori H, Teranishi T, Nakae Y, Seino Y, Miyake M and Yamada S 1999 Anomalous magnetic polarization effect of Pd and Au nano-particles *Phys. Lett.* A **263** 406–410
[19] Hurd C M 1966 The magnetic susceptibility of silver and gold in the range 6–300 k *J. Phys. Chem. Solids* **27** 1371–1374
[20] Crespo P, Litrán R, Rojas T C, Multigner M, de la Fuente J M, Sánchez-López J C, García M A, Hernando A, Penadés S and Fernández A 2004 Permanent magnetism, magnetic anisotropy, and hysteresis of thiol-capped gold nanoparticles *Phys. Rev. Lett.* **93** 087204
[21] Buchanan J D R, Hase T P A, Tanner B K, Chen P J, Gan L, Powell C J and Egelhoff W F 2002 Anomalously large intermixing in aluminum-transition-metal bilayers *Phys. Rev.* B **66** 104427
[22] Le Boit M G, Traverse A, Nvot L, Pardo B and Corno J 1988 Grazing x-ray reflectometry and rutherford backscattering: two complementary techniques for the study of thin film mixing *Nucl. Instrum. Methods Phys. Res. Section B: Beam Interact. Mater. Atoms* **29** 653–660
[23] Kowalik I A, Öhrwall G, Jensen B N, Sankari R, Wallén E, Johansson U, Karis O and Arvanitis D 2010 Description of the new i1 0 1 1 beamline for magnetic measurements using synchrotron radiation at max-lab *J. Phys.: Conf. Ser.* **211** 012030
[24] Carra P, Thole B T, Altarelli M and Wang X 1993 X-ray circular dichroism and local magnetic fields *Phys. Rev. Lett.* **70** 694–697
[25] Arac E, Burn D M, Eastwood D S, Hase T P A and Atkinson D 2012 Study of focused-ion-beam-induced structural and compositional modifications in nanoscale bilayer systems by combined grazing incidence x-ray reflectivity and fluorescence *J. Appl. Phys.* **111** 044324
[26] Mller W, Eckstein W and Biersack J P 1988 Tridyn-binary collision simulation of atomic collisions and dynamic composition changes in solids *Comput. Phys. Commun.* **51** 355–368
[27] Andersen H H 1979 Depth resolution of sputter profiling *Appl. Phys.* **18** 131–140
[28] Á Barna, Kotis L, Lábár J L, Osváth Z, Tóth A L, Menyhárd M, Zalar A and Panjan P 2007 Ion beam mixing by focused ion beam *J. Appl. Phys.* **102** 053513
[29] Zhang K, Lieb K P, Marszalek M, Milinovic V and Tokman V 2006 Ion beam mixing of Co/Fe multilayers: magnetic and structural properties *Thin Solid Films* **515** 700–704
[30] Tripathi J K, Kanjilal A, Rajput P, Gupta A and Som T 2009 Modification of the magnetic and the structural properties of Pt/Cr/Co multilayers by He+-ion irradiation *Nucl. Instrum. Methods Phys. Res. Section B: Beam Interact. Mater. Atoms* **267** 1608–1611
[31] Bland J A C, Padgett M J, Butcher R J and Bett N 1989 An intensity-stabilised He-Ne laser for measuring small magneto-optic kerr rotations from thin ferromagnetic films *J. Phys. E: Sci. Instrum.* **22** 308
[32] Savage D E, Kleiner J, Schimke N, Phang Y H, Jankowski T, Jacobs J, Kariotis R and Lagally M G 1991 Determination of roughness correlations in multilayer films for x-ray mirrors *J. Appl. Phys.* **69** 1411–1424
[33] Aldred A T 1966 Magnetization of iron-gallium and iron-arsenic alloys *J. Appl. Phys.* **37** 1344–1346
[34] Corb B W 1985 Magnetic moments and coordination symmetry in bcc Fe-M alloys *Phys. Rev.* B **31** 2521–2523
[35] Parra R E and Cable J W 1980 Neutron study of magnetic-moment distribution in Ni-Pt alloys *Phys. Rev.* B **21** 5494–5504
[36] Poulopoulos P *et al* 2001 X-ray magnetic circular dichroic magnetometry on Ni/Pt multilayers *J. Appl. Phys.* **89** 3874–3879
[37] Corb B W, O'Handley R C and Grant N J 1983 Chemical bonding, magnetic moments, and local symmetry in transition-metal–metalloid alloys *Phys. Rev.* B **27** 636–641
[38] Moghadam N Y, Stocks G M, Kowalewski M and Butler W H 2001 Effects of Ta on the magnetic structure of permalloy *J. Appl. Phys.* **89** 6886–6888
[39] Mitsuoka K, Miyajima H, Ino H and Chikazumi S 1984 Induced magnetic moment in ferromagnetic Fe alloys by tetragonally elongated lattice expansion *J. Phys. Soc. Japan* **53** 2381–2390
[40] Ray R and Hasegawa R 1978 Rapidly quenched metastable iron–boron solid solutions *Solid State Commun.* **27** 471–474
[41] Mirbt S, Abrikosov I A, Johansson B and Skriver H L 1997 Magnetic properties of fe embedded in V and Cr:ff thin films and dilute alloys *Phys. Rev.* B **55** 67–69
[42] Scherz A, Wende H, Poulopoulos P, Lindner J, Baberschke K, Blomquist P, Wäppling R, Wilhelm F and Brookes N B 2001 Induced V and reduced Fe moments at the interface of Fe/V(0 0 1) superlattices *Phys. Rev.* B **64** 180407
[43] Moruzzi V L, Marcus P M, Schwarz K and Mohn P 1986 Ferromagnetic phases of bcc and fcc Fe, Co, and Ni *Phys. Rev.* B **34** 1784–1791
[44] Cable J W and Wollan E O 1973 Magnetic-moment distribution in NiFe and AuFe alloys *Phys. Rev.* B **7** 2005–2016
[45] Uba L, Uba S, Antonov V N, Yaresko A N, Ślęzak T and Korecki J 2000 Magneto-optical anisotropy study of Fe_n/Au_n superlattices *Phys. Rev.* B **62** 13731–13747
[46] Jaouen N, Wilhelm F, Rogalev A, Goulon J, Ortega L, Tonnerre J M and Yaresko A 2008 Electronic and magnetic interfacial states of Ag in an $Ni_{81}Fe_{19}$/Ag coupled multilayer *J. Phys.: Condens. Matter* **20** 095005
[47] Jaouen N, Wilhelm F, Rogalev A, Tonnerre J-M, Johal T K and Van der Laan G 2005 Ag^- and W-induced magnetic moment in 3*d* multilayer *IEEE Trans. Magn.* **41** 3334–3336
[48] Wilhelm F, Poulopoulos P, Wende H, Scherz A, Baberschke K, Angelakeris M, Flevaris N K and Rogalev A 2001 Systematics of the induced magnetic moments in 5*d* layers and the violation of the third hund's rule *Phys. Rev. Lett.* **87** 207202
[49] Wilhelm F *et al* 2000 Layer-resolved magnetic moments in Ni/Pt multilayers *Phys. Rev. Lett.* **85** 413–416
[50] Guo G Y and Ebert H 1996 On the origins of the enhanced magneto-optical kerr effect in ultrathin Fe and Co multilayers *J. Magn. Magn. Mater.* **156** 173–174
[51] Zhang P and Sham T K 2003 X-ray studies of the structure and electronic behavior of alkanethiolate-capped gold nanoparticles: the interplay of size and surface effects *Phys. Rev. Lett.* **90** 245502
[52] Ding L, Qiu H, Li C, Xiang D, Teng J and Yu G 2013 Control of spin-polarized electron magnetoresistance in Ta/NiFe/Ta films by intercalation of Au *J. Phys. D: Appl. Phys.* **46** 025002